Journal of Microscopy, *Vol.* 154, *Pt* 3, *June* 1989, *pp.* 193–207.
Received 1 *July* 1988; *revised* 18 *November* 1988; *accepted* 30 *November* 1988

Theoretical study of the ultimate resolution of SEM

by DING ZE-JUN* *and* RYUICHI SHIMIZU, *Department of Applied Physics, Faculty of Engineering, Osaka University, Suita, Osaka* 565, *Japan*

KEY WORDS. SEM, secondary electron, ultimate resolution, contrast, probe size, edge-to-edge, Monte Carlo simulation.

SUMMARY

This work aims to clarify the problem of why the ultimate resolution assessed experimentally from the observation of 0·8 nm separation of Au–Pd fine particles is beyond the theoretical resolution limit of scanning electron microscopy (SEM). The correlation between the spatial distribution of secondary electrons on a sample surface and the resolution estimated by edge-to-edge separation in SEM was studied by a Monte Carlo simulation with secondary electron generation included. The result clearly indicates that the edge-to-edge separation can extend beyond the theoretical ultimate resolution, particularly by image processing for contrast expansion and by improving the signal to noise ratio (S/N).

INTRODUCTION

Development of high-brightness electron sources and progress in the electron optical designing of instruments have enabled the scanning electron microscope (SEM) to approach its ultimate resolution. This allows wide applications in various fields such as semiconductor device technology, biology, material science, etc. Tanaka *et al.* (1986) reported high-resolution observation of biological specimens coated with heavy metals. Furthermore, Nagatani & Saito (1986) demonstrated that a spatial resolution of 0·8 nm is attainable from the observation of edge-to-edge separation of Au–Pd fine particles evaporated on carbon substrate with the same type of SEM.

Regarding the resolution of SEM, it is well known that numerous factors are involved, such as the beam formation and the signal detection, which depend strongly on the instrument employed. As it is unrealistic to expect to obtain an image of higher spatial resolution than the probe diameter, efforts have been made to get a smaller probe size with sufficient current intensity for SEM observation. The use of the high-brightness field emission gun has contributed much to the attainment of high resolution. However, due to the limitation imposed by the aberrations, diffraction and source size the probe is limited to a certain size.

*On leave from: Fundamental Physics Center, China University of Science and Technology, Hefei, Anhui, People's Republic of China.

It has been proposed from electron optical designing that the minimum probe size of 0·6 nm or less is attainable with modern instruments at an accelerating voltage of 30 kV (Nagatani & Saito, 1986). Hence, the observation of 0·8 nm edge-to-edge resolution was believed to be an indication of such a probe size of 0·8 nm diameter or less. Crewe (1986) has mentioned briefly the probe size effect on the resolution. For detailed discussion on edge resolution and the optics of field emission gun SEM see Venables & Janssen (1980).

From a theoretical point of view, even if an electron beam with infinitesimal beam spot were achieved, the non-local interaction of the electron beam with the specimen causes the ejection of secondary electrons from points widely distributed around the incident point, known as interaction volume limitation. The full width at half maximum (FWHM) of the lateral distribution of secondary emission has been taken for the ultimate resolution of SEM.

Using Monte Carlo calculation, Shimizu & Murata (1971) pointed out that the ultimate resolution of SEM was restricted by the inelastic mean free path, λ. A simple diffusion model calculation (Everhart & Chung, 1972) and another Monte Carlo simulation of secondary electron generation in cascade processes (Koshikawa & Shimizu, 1974), agreed with this observation. The value of λ, for which the data have been compiled by Seah & Dench (1979) and tabulated by Powell (1984, 1985a), varies between 0·5 and 2 nm for metals and several times larger for insulating materials. Taking into account the spot size of an electron beam, d_p, a coarse estimation of the resolution can thus be given by $\sqrt{d_p^2 + \lambda^2}$, leading to the common feeling that the ultimate resolution of SEM is 1–2 nm, though the resolution depends on the features of a sample, such as topography of surface and material.

Experimentally, the check of the resolution of an apparatus has usually not been made by the observation of the flat surfaces as assumed in the theory but often by the observation of fine heavy metal particles on a light substrate to assure higher contrast in the SEM image. In this case the resolution is assessed by the minimum distance observable between two edges. It should be noted that this edge-to-edge resolution is somewhat different from the theoretical resolution defined above.

In this paper we point out that it is possible to get an edge-to-edge resolution better than the theoretical resolution, provided that a sufficient S/N is assured in the SEM images of the edges. A similar conclusion has been made by Catto & Smith (1973). The correlation among those factors such as probe size, beam current, detection efficiency, contrast and resolution has been widely discussed (e.g. Wells, 1974; Goldstein *et al.*, 1981; Reimer, 1985) and a recent Monte Carlo simulation of high resolution has been made by Joy (1988). The discrepancy that should exist between the theoretical and practical edge-to-edge resolutions, however, has not yet been fully discussed. Particularly, the recent experimental observation in high resolution requires a more quantitative explanation based on careful evaluation of all the parameters affecting the resolution.

The main purpose of the present study is, therefore, to answer the question of how the ultimate resolution assessed experimentally from the observation of a 0·8 nm separation of Au–Pd fine particles is beyond the theoretical resolution limit of SEM, by Monte Carlo simulation of the secondary electron generation and the contrast formation near the edges.

MODEL CALCULATION

Monte Carlo calculation, based on the simulation of trajectories of electrons and various scattering processes taking place in solids, is probably the best way to study the interaction of kilovolt primary electrons with solids, leading to the more comprehensive understanding of the different kinds of signal formation processes. Monte Carlo

simulation of electron trajectories essentially uses random numbers to decide the scattering angle, energy loss, step length, etc. Many of these simulation models have been proposed to describe the complicated scattering processes in solids under a certain approximation to obtain the information on various types of signals of interest (e.g. Green, 1963; Newbury & Yakowitz, 1976; Samoto & Shimizu, 1983; Desalvo *et al.*, 1984).

In this work we are particularly interested in secondary electrons as a signal for SEM images. The secondary electrons, with a probable energy about 2–3 eV above the vacuum level, are generated through the various inelastic scattering processes, e.g. valence electron excitation, core electron excitation and plasmon decay (Chung & Everhart, 1977), and through a cascade processes within a sample. Only those secondary electrons produced near the surface of the sample can reach the surface, and only those which maintain sufficient energy to overcome the surface barrier, can escape from the surface as true secondary electrons (Seiler, 1983). Some simulations have been performed on the basis of a secondary cascade model (Koshikawa & Shimizu, 1974; Ganachaud & Cailler, 1979) or combined with a diffusion model (Joy, 1987a; Suichu *et al.*, 1987) for studying the energy, angular and spatial distribution, as well as total yield of secondary emission. The increasing use of supercomputers allows the direct simulation of secondary electron generation in cascade processes which produce a huge number of secondary electrons within the sample.

The model adopted in this study is more comprehensive, allowing wider applications of the materials of known dielectric constants. Both the energy distributions of backscattered and secondary electrons obtained by this model agree very well with the experimental results (Ding & Shimizu, 1988; Ding *et al.*, 1988). The contribution of backscattered electrons to the production of secondary electrons is also included in the calculation. No classification is given to those secondary electrons produced either directly by primary electrons or by backscattered electrons. The details of the present Monte Carlo model are described below.

The total stopping power calculated by Tung *et al.* (1979) is used to evaluate stopping power due to valence electron excitation by

$$\left(\frac{\mathrm{d}E}{\mathrm{d}s}\right)_{\text{outer-shells}} = \left(\frac{\mathrm{d}E}{\mathrm{d}s}\right)_{\text{total}} - \sum_j \left(\frac{\mathrm{d}E}{\mathrm{d}s}\right)_j \qquad (1)$$

where j runs over all the directly simulated inner-shells, $3d_{3/2}$, $3d_{5/2}$, $4s_{1/2}$, $4p_{1/2}$ and $4p_{3/2}$, of an Au atom. Because of the limitation of memory space in a computer simulation, the deep inner-shells are not included in the direct excitations, due to their low excitation probabilities. Instead of the usual Bethe model of total stopping power, Tung's is used, as it is still valid in such lower energy regions of secondary electrons. The excitation of inner-shell electrons is represented by Gryzinski's (1965) equation for an electron with an energy above 160 eV. If it is unnecessary to assess a single excitation event of secondary electrons from outer-shells one may directly utilize the stopping power of outer-shells in the continuous slowing down approximation, i.e. assuming an electron continuously dissipates its energy along a step length between two collisions. However, the secondary electron excitation from outer-shells should not be omitted. We then treat the outer-shell electrons like the innter-shell electrons by extending Gryzinski's equation to such shells (Adesida *et al.*, 1980) in the sense that the total average energy loss due to such shells is the same as in Eq. (1). Two parameters of an effective shell, E_B and n_B, corresponding to mean binding energy and total number of electrons of outer-shells, can be obtained from Eq. (1). For Au, having numerous outer-shells, we tentatively represented those shells by two effective shells with E_B of 220 and 29 eV and n_B of 32 and 16, by best fitting to Eq. (1), regarding E_B

and n_B only as fitting parameters. Thus, the total inelastic scattering cross-section is given by

$$\sigma_{in} = \sum_i \sigma_i = \sum_i n_i \pi e^4 \frac{1}{E_i^2} \frac{E_i}{E} \left(\frac{E - E_i}{E + E_i}\right)^{3/2} \left\{1 + \frac{2}{3}\left(1 - \frac{E_i}{2E}\right) \ln\left[2{\cdot}7 + \left(\frac{E}{E_i} - 1\right)^{1/2}\right]\right\} \tag{2}$$

where E_i and n_i are the binding energy and number of electrons for inner-shells, equal to E_B and n_B for two effective shells, respectively. The associated excitation function is

$$\frac{d\sigma_i}{d(\Delta E)} = n_i \pi e^4 \frac{1}{(\Delta E)^3} \frac{E_i}{E} \left(\frac{E}{E + E_i}\right)^{3/2} \left(1 - \frac{\Delta E}{E}\right)^{E_i/(E_i + \Delta E)} \times \left\{\frac{\Delta E}{E_i}\left(1 - \frac{E_i}{E}\right) + \frac{4}{3} \ln\left[2{\cdot}7 + \left(\frac{E}{E_i} - 1\right)^{1/2}\right]\right\}. \tag{3}$$

Transferring of loss energy ΔE in a collision event to an electron in the excited shell produces a secondary electron.

In a low energy region, below a critical energy chosen to be 160 eV, the majority of secondary electrons is created through secondary cascade multiplication. This, then, requires a more accurate approach. The excitation function,

$$\frac{d\sigma_{in}}{d(\Delta E)} = \frac{me^2}{2\pi n\hbar^2} \frac{1}{E} Im\left[\frac{-1}{\varepsilon(\Delta E)}\right] \ln\left(\frac{cE}{\Delta E}\right) \tag{4}$$

where n is the atomic number density (cm^{-3}) and $\varepsilon(\Delta E)$ is a dielectric constant experimentally available from optical measurements, is employed to evaluate the loss energy ΔE in inelastic collision processes. The optical data compiled by Hagemann *et al.* (1975) were used. The inelastic mean free paths derived from Eq. (4), which satisfy the equation

$$\sigma_{in} = \frac{1}{n\lambda} = \int_0^{E - E_F} \frac{d\sigma_{in}}{d(\Delta E)} d(\Delta E) \tag{5}$$

with the fitting parameter c equal to 1·65, agree well with the experimental results down to Fermi energy E_F (Powell, 1985b; Ding & Shimizu, 1988) and also coincide with the results of Tung *et al.* (1979). Transferring of this ΔE to a Fermi electron creates a secondary electron. This approach is particularly useful for noble metals since the dielectric constant accurately describes the energy loss process due to numerous poorly defined outer-shells of a heavy atom in a solid. The critical energy, 160 eV, is decided by considering the energy dependence of λ. λ becomes smaller with decreasing energy, and reaches a minimum value at about 50–80 eV, indicating that below 160 eV the secondary cascade becomes important. The relation beween λ and cascade multiplication has been discussed by Joy (1987a). The dielectric approach is certainly applicable to high energy electrons; however, we have not found any significant difference on the secondary yield if a higher critical energy is chosen. An appropriate value is necessary for a finer tabulation interval of the excitation function and, hence, for a finer integration interval in Eq. (5).

For description of an elastic collision between an electron and an atom we use the Mott's differential cross-section,

$$\frac{d\sigma_{el}}{d\Omega} = |f(\theta)|^2 + |g(\theta)|^2 \tag{6}$$

where f and g are scattering amplitudes obtained from the partial wave expansion solution of Dirac's equation (Bunyan & Schonfelder, 1965), since the Rutherford formula commonly used is a poor approximation for heavy elements and in low-energy regions (Ichimura & Shimizu, 1981). The integration over all the entire solid angles gives the total elastic scattering cross-section,

$$\sigma_{el} = \int_0^{\pi} \frac{d\sigma_{el}}{d\Omega} 2\pi \sin\theta \, d\theta. \tag{7}$$

The total scattering cross-section is simply the sum,

$$\sigma_T = \sigma_{el} + \sigma_{in}. \tag{8}$$

As the detailed procedure for a Monte Carlo simulation has been reported in many papers (e.g. Shimizu *et al.*, 1976; Desalvo *et al.*, 1984; Valkealahti & Nieminen, 1984; Reimer & Stelter, 1986), we shall give only the essential elements here. The electron trajectory is followed by simulating randomly occurring scattering events. The distance, l, that an electron travels between two collisions is obtained from

$$l = (n\sigma_T)^{-1} \ln R_1 \tag{9}$$

where R_1 represents a uniform random number between 0 and 1. The next step is to determine the type of an individual scattering event by using another random number R_2. It is elastic provided,

$$R_2 < \sigma_{el}/\sigma_T. \tag{10}$$

Above 160 eV it is necessary to determine a shell at which the excitation happens when the collision is inelastic. Such a shell is the ith if the equation,

$$\frac{\sum_m^{i-1} \sigma_m}{\sigma_{in}} < R_3 < \frac{\sum_m^{i} \sigma_m}{\sigma_{in}} \tag{11}$$

where $\sigma_0 = 0$, is satisfied. The energy loss, ΔE, and the energy of the excited secondary electron, E_2, are found from,

$$R_4 = \int_{E_i}^{\Delta E} \frac{d\sigma_i}{d(\Delta E')} d(\Delta E')/\sigma_i \qquad E_2 = \Delta E - E_i \quad (E > 160\,\text{eV}) \tag{12}$$

and,

$$R_4 = \int_0^{\Delta E} \frac{d\sigma_{in}}{d(\Delta E')} d(\Delta E')/\sigma_{in} \qquad E_2 = \Delta E + E_F \quad (E < 160\,\text{eV}). \tag{13}$$

The probability for scattering into the azimuthal angle, ϕ, is uniformly distributed and selected by

$$\phi = 2\pi R_5. \tag{14}$$

We determine the scattering angle θ through the relation,

$$R_6 = \int_0^{\theta} \frac{d\sigma_{el}}{d\Omega} 2\pi \sin\theta' d\theta'/\sigma_{el} \tag{15}$$

for elastic scattering and the angle of deflection θ by

$$\sin^2\theta = \frac{\Delta E}{E} \tag{16}$$

for inelastic scattering. The coordinates and energy of the scattering electron can then be decided. This completes a scattering event and repeating the steps (9)–(16) forms an electron trajectory.

Once a secondary electron is generated by a primary electron in an excitation event, its energy, coordinates and moving direction are stored. After finishing tracing the primary electron the stored information on the secondary electron is recalled and the trajectories are simulated in the same way as for a primary electron. A large number of low-energy secondary electrons are then successively generated. This cascade process is traced until all the electrons either escape from the surface as true secondary electrons or come to rest within the sample. The refraction of slow electrons by the potential barrier at the surface when they leave the sample (Koshikawa & Shimizu, 1974) was also taken into account.

As a boundary condition in the Monte Carlo simulation, which defines the shape of the sample, we assumed that the sample was composed of an Au film 10 nm thick with sharp edges separated by a narrow gap. This demonstrates a practical sample, the fine Au–Pd particles on carbon substrate or biological samples coated with heavy metals, adopted for the observation of the resolution limit of an SEM apparatus. Since the elastic scattering cross-section for a carbon substrate is much smaller than that for heavy metals, the influence of backscattering from the substrate can be neglected. Furthermore, the secondary electrons emitted from the substrate facing the gap can also be neglected because of very low yield of secondary electrons. The penetration effect at sharp edges (Wells, 1978) is negligible since we are dealing with the case of normal incidence of electrons of several tens of kilovolts.

To obtain the contrast of an SEM image near the edges, which is a type of topographical contrast, the secondary yield at the different incident position is calculated with a zero diameter probe, resulting in the line scan profile $S_0(x)$ across the gap. All the electrons emitted from upper and side surfaces with energy less than 50 eV are counted to produce the secondary yield. In this way the edge effect is directly calculated against by a diffusion model (Matsukawa & Shimizu, 1974; Joy, 1987b). Then for a probe of finite size, assuming Gaussian intensity distribution of the primary beam,

$$G(x, y) = \frac{1}{2\pi\sigma^2} \exp\left(-\frac{x^2 + y^2}{2\sigma^2}\right), \tag{17}$$

the line scan profile is obtained as a convolution result using Gaussian function as a weight,

$$S(x') = \iint_{-\infty}^{+\infty} S_0(x) G(x - x', y)\, \mathrm{d}x\mathrm{d}y \tag{18}$$

where σ is the standard deviation.

RESULTS AND DISCUSSION

The calculations were performed at different positions from the edge using normal incidence of 30 kV primary electrons impinging on a 10-nm thick Au film. A calculation for 10 kV primary electrons incident on the Au film far from the edge was also done for comparison. 80,000–200,000 trajectories of primary electrons were used for each simulation performed with a supercomputer SX-1 of Osaka University. In Fig. 1 the trajectories of 200–400 primary electrons and of secondary electrons generated by those primary electrons are plotted for an incident point, 0·5 nm from the edge.

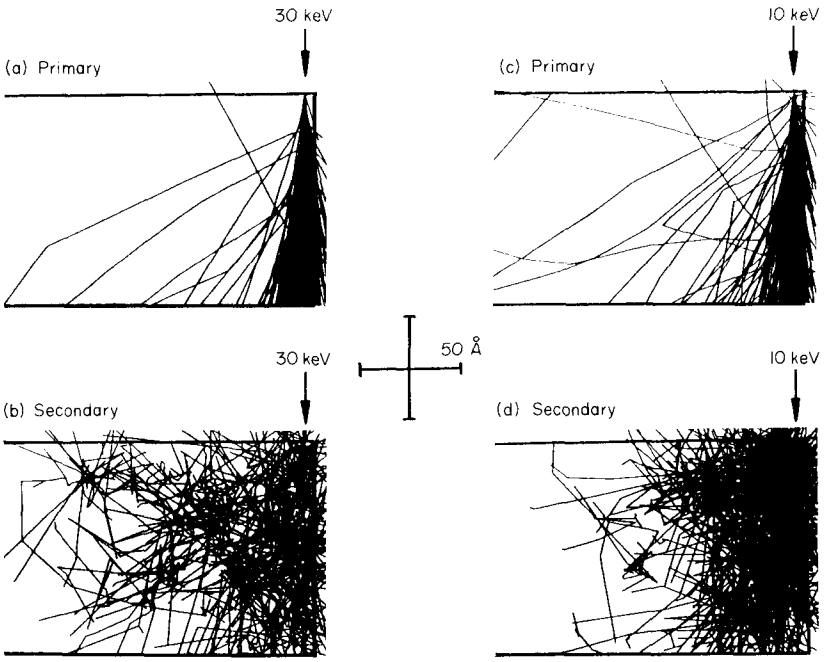

Fig. 1. Trajectories of electrons produced by a primary beam of infinitesimal spot size incident upon an Au film of 10 nm thickness a distance 0·5 nm from the edge: (a) for 400 primary electrons of 30 kV and (b) for their resulting secondary electrons; (c) for 200 primary electrons of 10 kV and (d) for their resulting secondary electrons.

Spatial distribution of secondary emission

First, we shall study the spatial distribution of secondary electron emission to see how a theoretical ultimate resolution should be defined. Fig. 2 shows that the radial intensity distribution $I(r)$ per unit area and a normalized profile of secondary current emitted inside a circle of radius r,

$$I'(r) = \int_0^r r'\mathrm{d}r'I(r') / \int_0^\infty r'\mathrm{d}r'I(r') \tag{19}$$

together with its integrand is also demonstrated. Both the shapes of $I(r)$ and $I'(r)$ are very similar to those of a simple analytical calculation (Everhart & Chung, 1972). It is seen that the secondary emission is very intensive near the impact point and the maximum is $I(0)$. The diameter $2R_0$ at $I(R_0) = I(0)/2$ is often referred to as an estimation of resolution. In the present case both 30 and 10 kV electrons give a value of 0·8 nm. However, it should be noted that within a circle of radius R_0 only about 8% of the total current is contained. This is because with lower r the emission area $r\mathrm{d}r$ decreases. So the contribution of those secondary electrons emitted from the area greater than R_0 from the incident point should not be omitted. A reasonable radial resolution should be defined as a diameter, $d_r = 2R$, in which 50% of the current is contained, at least, $I'(R) = I'(\infty)/2$. From Fig. 2 the value of d_r is estimated to be 3·4 and 4·4 nm for the 30 and 10 keV primary energies, respectively.

For obtaining an image the electron probe is scanned in one direction (such as the x-axis) across a sample within a period of one line scan. The lateral distribution of secondary electron emission is, therefore, more important than radial distribution due

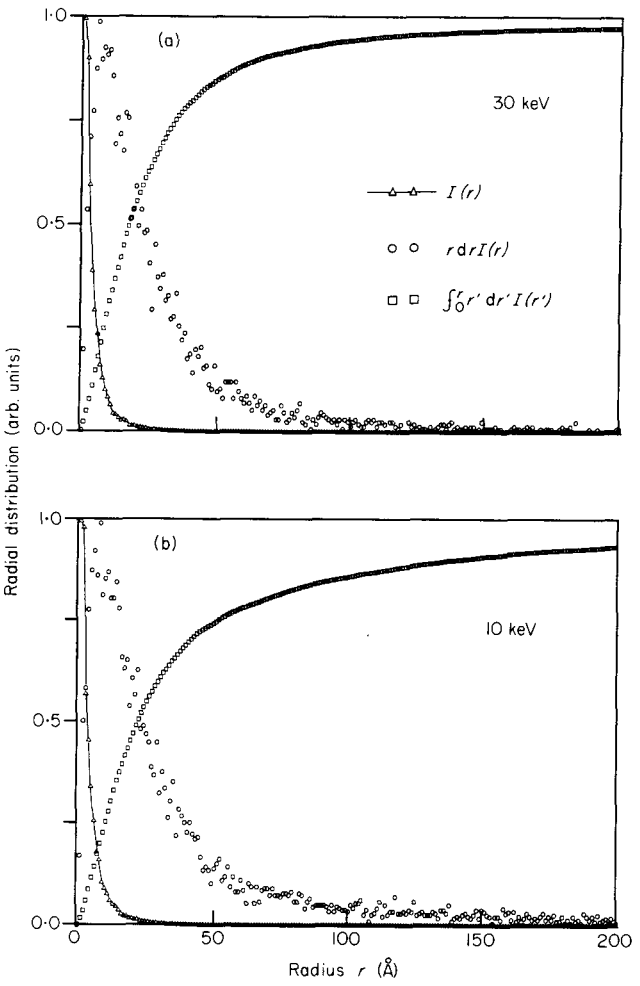

Fig. 2. Calculated relative radial distribution of secondary emission plotted against the radius r from the impact point. (△—△) The radial intensity distribution at r; (○) the secondary electron current emitted into a ring of radius r and of width dr, which are the numbers directly counted from a Monte Carlo simulation; (□) a normalized profile of secondary electron current emitted inside a circle r. (a) For 30 kV primary electrons and (b) for 10 kV primary electrons.

to its emphasis on the change of information along a special direction and its relation to a practical contrast. The lateral and radial distributions are related by

$$D(x) = \int_{-\infty}^{+\infty} I(\sqrt{x^2 + y^2})\, \mathrm{d}y. \tag{20}$$

Fig. 3 illustrates $D(x)$ derived directly in the same simulation as for the calculation of $I(r)$. We found that it can be well represented by a Laplacian distribution

$$L(x) = \frac{1}{\pi x_0[1 + (x/x_0)^2]} \tag{21}$$

with a $2x_0$, the FWHM, of 2·2 nm in this case. Following the discussion given above we also define the resolution of lateral distribution to be the distance d_x so that 50%

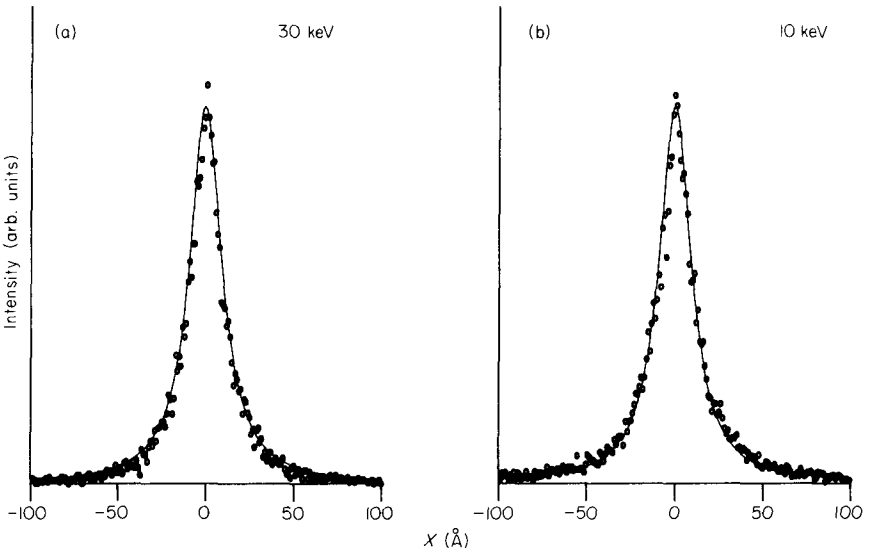

Fig. 3. Lateral distribution of secondary emission plotted against the distance from the impact point. Circles represent the calculated distribution and solid line the Laplacian distribution with FWHM of 2·2 nm. (a) For 30 kV primary electrons and (b) for 10 kV primary electrons.

of the total current is contained within it. For a $D(x)$ of exact Laplacian, d_x should be equal to FWHM. To check this we plotted the integrated intensity profile,

$$D'(x) = \int_{-\infty}^{x} D(x')\,dx' \Big/ \int_{-\infty}^{+\infty} D(x')\,dx' \tag{22}$$

in Fig. 4. The distance between the 25 and 75% points on $D'(x)$ is the measure of d_x. Its values are 2 and 2·3 nm for 30 and 10 keV primary energies, respectively. The FWHM (Sparrow criterion) of $D(x)$ can then equal d_x as long as d_x is evaluated from $D'(x)$.

We now consider the Rayleigh criterion which states that two points a distance d_R apart will be resolved when their distributions overlap at half their separation with an intensity drop of 75% of the maximum intensities (Reimer, 1985). It can then be evaluated from the overlapped profile by two Laplacian lateral distributions with FWHM of d_x,

$$L(-d_R/2) + L(d_R/2) = 0{\cdot}75[L(0) + L(d_R)], \tag{23}$$

leading to the result of $d_R \simeq 1{\cdot}14d_x$. We then get values of Rayleigh resolution being about 2·3 and 2·6 nm for 30 and 10 keV primary energies, respectively. It should be noted that the Rayleigh criterion was originally used for human eye detection and it gives a value poorer than from modern signal acquisition and processing systems. A similar situation in scanning Auger electron microscopy has been recently discussed by Cazaux (1987) and Cazaux *et al.* (1988).

In conclusion the ultimate theoretical resolution, interrelating the spatial emission of secondary electrons independently of beam size, can be set as 2 nm. This result coincides with the one of conventional coarse estimation. However, this value cannot be regarded as the limit since a modern signal processing system may allow SEM to exceed the Sparrow and Rayleigh criterions.

It is seen, even though $I(r)$ and $D(x)$ do not show marked difference in the resolution for different energies, that the integrated profile $I'(r)$ and $D'(x)$ can reveal an obvious

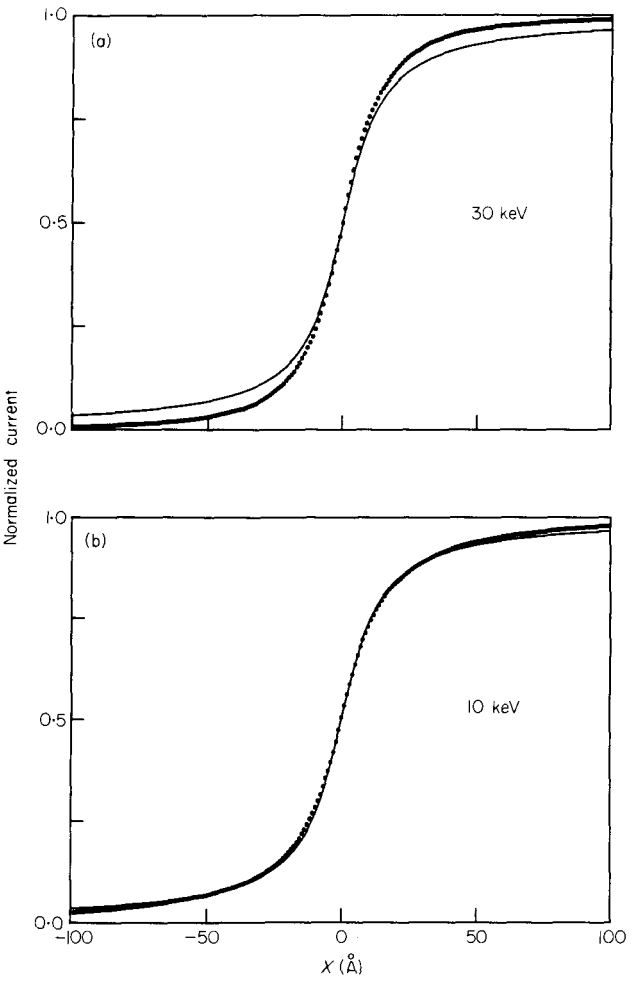

Fig. 4. Lateral distribution of secondary electron current integrated from infinity to the distance from the impact point. Circles represent the calculated profile and solid line that deduced from a Laplacian distribution with FWHM of 2·2 nm. (a) For 30 kV primary electrons and (b) for 10 kV primary electrons.

difference. The tendency to poorer resolution with decreasing primary energy, due to the spreading of the primary beam in the sample, has been pointed out by Joy (1985). For a bulk Au sample the tails of $I(r)$ and $D(x)$ may be increased compared to the present case by the contribution of the backscattering effect. However, these secondary electrons do not play any significant role in the present study since they are distributed over a much wider area of micrometres and form only a flat background [discussed in detail elsewhere (Shimizu & Murata, 1971)].

Edge-to-edge resolution

The edge effects of secondary electron emission are shown in Fig. 5, calculated from Monte Carlo simulations for a 30 kV electron beam of infinitesimal spot size. Far from the edge the signal intensity is nearly constant and rises to a maximum near the edge, resulting in so-called edge contrast. This behaviour should depend on the target sample through the correlation between the mean attenuation length and the material

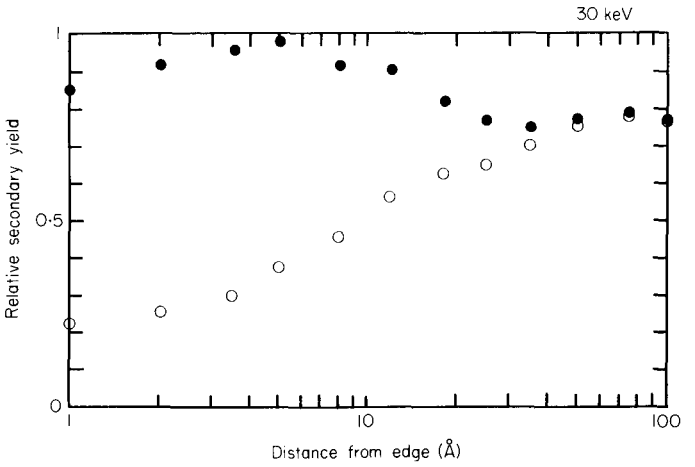

Fig. 5. The relative secondary yield against the distance measured from the incident point to an edge of the 10-nm thick Au film, obtained from the Monte Carlo calculations. (○) The yield for which only those secondary electrons emitted from the upper plane are included, and (●) for secondary electrons emitted from both the upper plane and the side surface.

(Matsukawa & Shimizu, 1974). If a sample is comparable with an electron probe in size and is smaller than the interaction volume, the edge brightness in a micrograph may disappear (Joy, 1984). But if a sufficiently high contrast between the edges was assured, a higher resolution observation is attainable as discussed below.

Before discussing the convolution result for a certain value of probe size of electron beam the definition of this probe diameter should be given. As pointed out by Michael & Williams (1987), due to the various definitions of the aberration discs and the initial Gaussian diameter, the calculated probe diameter actually represents some unknown fraction of the total probe current contained and, hence, it is difficult to compare an experimentally measured probe diameter directly with the calculated one. Furthermore, the very fine electron probe may not be Gaussian (Venables & Janssen, 1980; Cliff & Kenway, 1982). Several definitions of a diameter are, assuming Gaussian distribution, taken conventionally as, for example a single standard deviation σ, FWHM or full width at tenth maximum (FWTM), for which about 40, 50 and 90% of the total current is contained, respectively. Hereafter we choose FWHM as the definition of diameter d_p even though FWTM may be more appropriate as suggested by Michael & Williams (1987). Conversion to the other definitions of the diameter can be easily done using $0{\cdot}85d_p$ and $1{\cdot}82d_p$ for σ and FWTM, respectively.

The line scan profiles $S(x)$ are calculated for an electron probe of several finite sizes by the convolution procedure described in (18). Figure 6(a) shows $S(x)$ formed by a beam scanning across the gap between edges for different probe sizes. It is difficult to set a contrast scale for converting a calculated line scan profile to an image, particularly, due to a non-linear transformation of signals from the detected current to the brightness in a micrograph. Therefore, direct comparison between the calculated contrast and experiment should not be made. Hereafter, we use the FWHM of $S(x)$ as a criterion for the observable edge-to-edge resolution.

There are two possibilities for the observation of a 0·8-nm edge-to-edge resolution in an image. The first is the case that both d_p and gap separation, s, are less than 0·8 nm. From the natural contrast, 0·8 nm of FWHM of $S(x)$ can be obtained for 0·5 nm of d_p and of s as shown in Fig. 6(a). The deterioration of the edge-to-edge resolution is, in

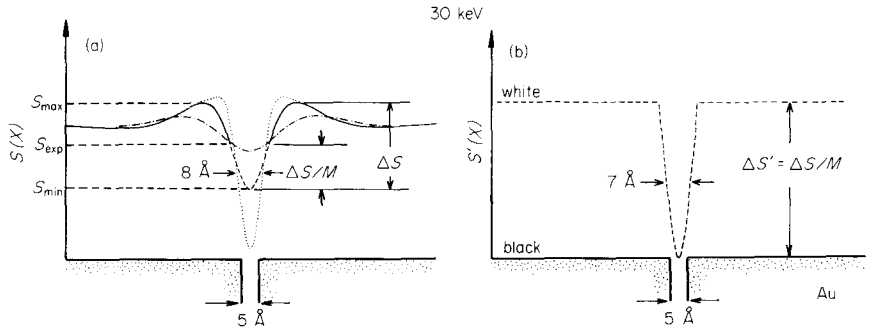

Fig. 6. The line scan profiles near the edges for several probe diameters, d_p. (a) $S(x)$ for natural contrast, (b) $S'(x)$ for expanded contrast, as shown for d_p of 1 nm with an expansion constant, $M = 2$.

this case, due to the escape depth of secondary electrons. Note that the deterioration is not so large as that for flat surfaces often discussed so far, leading to the possibility that the edge-to-edge resolution can be less than 1 nm for an electron probe of several ångströms diameter.

There is, however, another possibility for obtaining such a high edge-to-edge resolution. Here we consider d_p is comparable with, or greater than, 0·8 nm. The edge resolution from a natural contrast is always larger than 0·8 nm. But some devices may enable the higher resolution to be attained by the image processing: the simplest one is that, for instance, one adjusts the contrast by controlling the black and white levels in practical SEM operation. If the setting of the contrast levels is adjusted so that only the top section of the peak of $S(x)$ is used to form the contrast of the SEM image, the gap is to be observed with the effective profile $S'(x)$ being expanded as depicted in Fig. 6(b). Therefore, the edge-to-edge resolution will be improved, enabling the SEM observation to be made with such a resolution as if the spot size of the electron probe were reduced to less than the gap separation. This fact has already been pointed out by Venables & Janssen (1980) and a good example of this kind of image analysis has been reported by McMillan *et al.* (1987) in the limiting case for S/N being extremely large.

There is certainly a limitation for expanding the contrast of an SEM image since the image will become increasingly noisy for larger contrast expansions, and at a certain level will be too blurred to be tolerable. We can then estimate the maximum contrast expansion constant,

$$M = \Delta S/\Delta S' \tag{24}$$

where $\Delta S(= S_{max} - S_{min})$ is the variation of the signal resulting in the contrast and $\Delta S'(= S_{exp} - S_{min})$ the effective signal variation after an expansion, with S_{max}, S_{min} and S_{exp} denoting maximum, minimum and an appropriate value between S_{max} and S_{min}, of $S(x)$, as illustrated in Fig. 6(a). Here, 'contrast expansion' means that the ΔS in the natural contrast is expanded by M to $\Delta S'$ in the expanded contrast where the black and white levels are set to S_{min} and S_{exp}, respectively.

M should be determined from the threshold equation, which describes the relation between the total S/N and the minimum probe current required to form an SEM image (Wells, 1974; Reimer, 1985). The noise is statistical fluctuations of the signal-carrying quanta, originated at every step of the signal transformation processes. The total S/N is dominated by the one at the noise bottleneck, at which the signal quanta is minimum in the signal pass, of the system. This is the point where the primary

electrons are converted to the detectable secondary electrons but with low efficiencies due to the low secondary yield and low capture efficiency of the detector compared with the high conversion efficiency of the scintillator and photomultiplier. Hence, the total S/N of the system, which is directly assessed from Fig. 6 as $S_{max}/\sqrt{S_{max}}$ ($=\sqrt{S_{max}}$), can be approximated as,

$$S/N = 1/\sqrt{1/n_p + 1/n_s} \tag{25}$$

where n_p and n_s are the mean numbers of primary electrons incident on the sample and of the secondary electrons attracted into a detector within a certain time of observation, respectively. Considering that a beam with current 10^{-12} A scans over the sample within 200 s to produce an image on one frame of 500 × 500 pixels, n_p is about 5×10^3 per pixel. The secondary yield of Au at 30 keV is nearly 0·2. Taking into account the detection efficiency we estimated the detectable secondary yield to be 0·1. n_s is thus about 5×10^2 per pixel. The S/N of a natural contrast being nearly equal to 20.

By Rose criterion one can discern the difference between two points in a scanned TV image only if the signal change exceeds the noise N by a factor of five $\Delta S' > 5N$. If an image is recorded on a film the smaller factor may be permissible. Hence, we have

$$M < \frac{\Delta S}{5N} = \frac{(1-\alpha)S_{max}}{5\sqrt{S_{max}}} = \frac{1}{5}(1-\alpha)\frac{S}{N} \simeq 4(1-\alpha) \tag{26}$$

with $\alpha = S_{min}/S_{max}$. The values of α and M estimated from Fig. 6 for d_p of 1 nm and s of 0·5 nm are 0·44 and 2·2, respectively, leading to an estimation of the maximum edge-to-edge resolution (FWHM) of the expanded contrast of 0·7 nm in this case. This, therefore, suggests that with a maximum expansion constant an edge-to-edge resolution better than 0·8 nm is attainable even with an electron probe with spot size larger than 0·8 nm.

Improved resolution can be obtained with increased expansion constants. However, this may not be easily satisfied in practice because one cannot concentrate only on the resolution of one particular particle but on the moderate balance among S/N, contrast, resolution and brightness of the whole image.

The results discussed above are somewhat surprising. If we consider the Rayleigh criterion for lateral distribution in the limiting case, two points a distance d'_R apart do not show any dip in the total intensity at the mid-point between them. So in this case the two points are indistinguishable by any means of image processing. Replacing 0·75 in Eq. (23) by 1 we get $d'_R \simeq 0{\cdot}71 d_x$. The minimum value of d'_R is 1·4 nm. However, such consideration is based on the calculation for a plane surface. The emission of greater numbers of secondary electrons takes place at a sharp edge, which has two surfaces for electron ejection, and this produces a high edge-to-edge resolution. In this case the lateral distribution of secondary emission is nevertheless a kind of Laplacian, since $D(x)$ is abruptly increased to a large value $a(u)$, which depends on the distance u from the impact point to the edge, at a sharp edge,

$$D(x) = L(x)\theta(u-x) + a(u)\delta(u-x) \tag{27}$$

where $\theta(x)$ and $\delta(x)$ are step function and Dirac function, respectively [$\theta(x) = 1$ for $x > 0$, otherwise $\theta(x) = 0$; $\delta(x) = \infty$ for $x = 0$, otherwise $\delta(x) = 0$]. It is clear from Fig. 5 that if the secondary emission from the side surface is omitted such a high resolution is then unattainable.

There should be some limitations for the discussion on the possibility of high edge-to-edge resolution given above. With decreasing gap between two edges it becomes a problem as to whether or not those secondary electrons emitted from the side plane facing the gap will feel an electric field to be attracted by a detector. Furthermore, the penetration effect at edges cannot then be omitted.

Consequently, it has been seen that the edge-to-edge resolution depends on many factors of an experiment and can be improved by appropriate image processing to reduce the noise. However, there is a finite possibility that such a processing may lead to the artefact observation. Hence, it is strongly recommended that the experimentalist should be careful to assess the resolution and the probe size from the SEM observation.

CONCLUSION

We studied the spatial emission of secondary electrons by Monte Carlo simulations. The relationships between contrast, resolution and diameter are investigated theoretically. Discussion on the various definitions of resolution and of probe size are given. A theoretical ultimate lateral resolution, concerning only the interaction volume of secondary electron signal formation and the spatial distribution of secondary electron emission from an infinite plane surface, is estimated to be 2 nm. However, an edge resolution better than 0·8 nm is possible due to the edge effect. Furthermore, for a larger electron probe this resolution can also be achieved by contrast expansion and signal processing.

ACKNOWLEDGMENTS

The authors are very grateful to Professor K. Tanaka for drawing their attention to this question and to Dr T. Nagatani for providing the original SEM micrograph of 0·8 nm resolution. Thanks are also due to Dr O. C. Wells for helpful comments on the present work and Professor D. C. Joy for reviewing the manuscript.

REFERENCES

Adesida, I., Shimizu, R. & Everhart, T.E. (1980) A study of electron penetration in solids using a direct Monte Carlo approach. *J. Appl. Phys.* **51,** 5962–5969.

Bunyan, P.J. & Schonfelder, J.L. (1965) Polarization by mercury of 100 to 2000 eV electrons. *Proc. Roy. Soc.* **85,** 455–462.

Catto, C.J.D. & Smith, K.C.A. (1973) Resolution limits in the surface scanning electron microscope. *J. Microsc.* **98,** 417–435.

Cazaux, J. (1987) Some consideration of the lateral resolution in Auger electron spectroscopy. *J. Microsc.* **145,** 257–273.

Cazaux, J., Chazelas, J., Charasse, M.N. & Hirtz, J.P. (1988) Line resolution in the sub-ten-nanometer range in SAM. *Ultramicroscopy*, **25,** 31–34.

Chung, M.S. & Everhart, T.E. (1977) Role of plasmon decay in secondary electron emission in the nearly-free-electron metals-application to aluminum. *Phys. Rev.* **B15,** 4699–4715.

Cliff, G. & Kenway, P.B. (1982) The effects of spherical aberration in probe-forming lenses on probe size, image resolution, and X-ray spatial resolution in scanning transmission electron microscopy. In: *Microbeam Analysis–1982* (ed. by Heinrich, K.F.J.), pp. 107–110, San Francisco Press, San Francisco.

Crewe, A.V. (1986) Is there a limit to the resolving power of the SEM. In: *Proc. XIth Int. Cong. on Electron Microscopy*, Vol. 3, (ed. by T. Imura, S. Maruse and T. Suzuki), pp. 2105–2108. Jpn. Soc. Elect. Microsc., Tokyo.

Desalvo, A., Parisini, A. & Rosa, R. (1984) Monte Carlo simulation of elastic and inelastic scattering of electrons in thin films. I. Valence electron losses. *J. Phys. D: Appl. Phys.* **17,** 2455–2471.

Ding, Z.-J. & Shimizu, R. (1988) Monte Carlo study of backscattering and secondary electron generation. *Surf. Sci.* **197,** 539–554.

Ding, Z.-J., Shimizu, R., Sekine, T. & Sakai, Y. (1988) Theoretical and experimental studies of N(E)-spectra in Auger electron spectroscopy. Proc. 4th Intern. Conf. on Solid Films and Surfaces, *Appl. Surf. Sci.* **33/34,** 99–106.

Everhart, T.E. & Chung, M.S. (1972) Idealized spatial emission distribution of secondary electrons. *J. Appl. Phys.* **43,** 3707–3711.

Ganachaud, J.P. & Cailler, M. (1979) A Monte Carlo calculation of the secondary electron emission of normal metals. *Surf. Sci.* **83,** 498–530.

Goldstein, J., Newbury, D.E., Echlin, P., Joy, D.C., Fiori, C. & Lifshin, E. (1981) *Scanning Electron Microscopy and X-ray Microanalysis*, Plenum Press, New York.

Green, M. (1963) A Monte Carlo calculation of the spatial distribution of characteristic X-ray production in a solid target. *Proc. Phys. Soc.* **85,** 204–215.

Gryzinski, M. (1965) Classical theory of atomic collisions. I. Theory of inelastic collisions. *Phys. Rev.* **138,** A336–A358.

Hagemann, H.-J., Gudat, E. & Kunz, C. (1975) Optical constants from the far infrared to the X-ray region: Mg, Al, Cu, Ag, Au, Bi, C and Al_2O_3. *J. Opt. Soc. Am.* **65,** 742–744.

Ichimura, S. & Shimizu, R. (1981) Backscattering correction for quantitative Auger analysis. *Surf. Sci.* **112,** 386–408.

Joy, D.C. (1984) Beam interactions, contrast and resolution in the SEM. *J. Microsc.* **136,** 241–258.

Joy, D.C. (1985) Resolution in low voltage scanning electron microscopy. *J. Microsc.* **140,** 283–292.

Joy, D.C. (1987a) Model for calculating secondary and backscattered electron yields. *J. Microsc.* **147,** 51–64.

Joy, D.C. (1987b) Image simulation for the SEM. In: *Microbeam Analysis – 1987* (ed. by Geiss, R. H.), pp. 105–109, San Francisco Press, San Francisco.

Joy, D.C. (1988) Simulation of high-resolution SEM images. In: *Microbeam Analysis – 1988* (ed. by D. E. Newbury), pp. 143–148. San Francisco Press, San Francisco.

Koshikawa, T. & Shimizu, R. (1974) A Monte Carlo calculation of low-energy secondary electron emission from metals. *J. Phys. D: Appl. Phys.* 7, 1303–1315.

Matsukawa, T. & Shimizu, R. (1974) A new type edge effect in high resolution scanning electron microscopy. *Jpn. J. Appl. Phys.* **13,** 583–586.

McMillan, P.J., Yakush, A., Frykman, G., Nava, P.B. & Ras, V.R. (1987) Minima equalization – a useful strategy in automatic processing of microscopic images. *J. Microsc.* **148,** 253–262.

Michael, J.R. & Williams, D.B. (1987) A consistent definition of probe size and spatial resolution in the analytical electron microscope. *J. Microsc.* **147,** 289–303.

Nagatani, T. & Saito, S. (1986) Instrumentation for ultra high resolution scanning electron microscopy. In: *Proc. XIth Int. Cong. on Electron Microscopy*, Vol. 3 (ed. by T. Imura, S. Maruse and T. Suzuki), pp. 2101–2104. Jpn. Soc. Elect. Microsc., Tokyo.

Newbury, D.E. & Yakowitz, H. (1976) Studies of the distribution of signals in the SEM/EPMA by Monte Carlo electron trajectory calculations. *NBS Special Publication* **460,** 15–44.

Powell, C.J. (1984) Inelastic mean free paths and attenuation lengths of low-energy electrons in solids. In: *Scanning Electron Microscopy*, Vol. 4 (ed. by R. P. Becker), pp. 1649–1664, SEM Inc., Chicago.

Powell, C.J. (1985a) The energy dependence of electron attenuation lengths. *Surface Interface Anal.* 7, 256–262.

Powell, C.J. (1985b) Calculations of electron inelastic mean free paths from experimental optical data. *Surface Interface Anal.* 7, 263–274.

Reimer, L. (1985) *Scanning Electron Microscopy*, Springer-Verlag, Berlin.

Reimer, L. & Stelter, D. (1986) Fortran 77 Monte-Carlo program for minicomputers using Mott cross-sections. *Scanning*, **8,** 265–277.

Samoto, N. & Shimizu, R. (1983) Theoretical study of the ultimate resolution in electron beam lithography by Monte Carlo simulation, including secondary electron generation: energy dissipation profile in polymethyacrylate. *J. Appl. Phys.* **54,** 3855–3859.

Seah, M.P. & Dench, W.A. (1979) Quantitative electron spectroscopy of surfaces: a standard data base for electron inelastic mean free paths in solids. *Surf. Interface Anal.* 1, 2–11.

Seiler, H. (1983) Secondary electron emission in the scanning electron microscope. *J. Appl. Phys.* **54,** R1–R18.

Shimizu, R., Kataoka, Y. & Ikuta, T. (1976) A Monte Carlo approach to the direct simulation of electron penetration in solids. *J. Phys. D: Appl. Phys.* **9,** 101–114.

Shimizu, R. & Murata, K. (1971) Monte Carlo calculations of the electron–sample interactions in the scanning electron microscope. *J. Appl. Phys.* **42,** 387–394.

Suichu, L., Yongsheng, Z. & Ziqin, W. (1987) A Monte Carlo calculation of secondary electrons emitted from Au, Ag and Cu. *J. Microsc.* **148,** 289–295.

Tanaka, K., Mitsushima, A., Kashima, Y. & Osatake, H. (1986) A new high resolution scanning electron microscope and its application to biological materials. In: *Proc. XIth Int. Cong. on Electron Microscopy*, Vol. 3 (ed. by T. Imura, S. Maruse and T. Suzuki), pp. 2097–2100. Jpn. Soc. Elect. Microsc., Tokyo.

Tung, C.J., Ashley, J.C. & Ritchie, R.H. (1979) Electron inelastic mean free paths and energy losses in solids. *Surf. Sci.* **81,** 427–439.

Valkealahti, S. & Nieminen, R.M. (1984) Monte Carlo calculation of keV electron and positron slowing down in solids. II. *Appl. Phys. A*, **35,** 51–59.

Venables, J.A. & Janssen, A.P. (1980) Performance of a field emission gun scanning electron microscope column. *Ultramicroscopy*, **5,** 297–315.

Wells, O.C. (1974) *Scanning Electron Microscopy*, McGraw-Hill, New York.

Wells, O.C. (1978) Penetration effect at sharp edges in the scanning electron microscope. *Scanning*, **1,** 58–62.